Chapter 2
Piezoelectricity and Energy Harvester Modelling

The direct piezoelectric effect is well-suited for harnessing environmental vibrations and to convert them into usable electrical energy. Coated on a cantilever beam, piezoelectric ceramics allows simple energy harvesting without additional mechanical structures. In addition, relatively small external excitations result in output voltages of several volts which do not require low-efficient startup mechanisms as known from thermoelectric generators. In order to give the reader a feeling about what is important for developing interface circuitry for piezoelectric energy harvesters, the basics of piezoelectricity and its usage in energy harevsting are presented in this chapter. After the physical conversion principle has been introduced roughly, its application in cantilever beam harvesters is explained. The last two sections are about the modeling of kinetic, vibration based energy harvesters in general and piezoelectric energy harvesters in particular. Electrical equivalent circuits of the energy harvesters are essential for the simulation of entire energy harvesting systems composed of the mechanical harvester structure and the electrical interface circuitry on one hand, and on the other hand to understand their behavior by means of analytical calculations.

2.1 Theoretical Background of the Piezoelectric Effect

The theoretical treatment of the piezoelectric effect presented in this section is intentionally kept very superficial, because this book's focus is on the interface circuitry for piezoelectric energy harvesters, not the harvesters themselves. Nevertheless, the reader gets a basic introduction to this topic in order to be able to understand the challenges linked with energy extraction out of piezoelectric energy harvesters. A more thorough analysis of piezoelectricity can be found in [7].

T. Hehn and Y. Manoli, *CMOS Circuits for Piezoelectric Energy Harvesters*,
Springer Series in Advanced Microelectronics 38, DOI 10.1007/978-94-017-9288-2_2

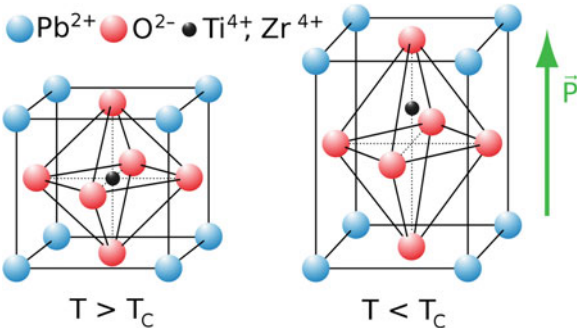

Fig. 2.1 Intrinsic piezoelectric effect in lead zirconate, showing the a crystallite above and below the Curie temperature T_C, where the charged zirconium or titanium ion moves relative to the center position

2.1.1 History and Conversion Principle

Certain solid materials like crystals and ceramics with no inversion symmetry [5] generate charges under an externally applied force. This so-called direct piezoelectric effect was initially discovered by the brothers Pierre Curie and Jacques Curie in the year 1880 and demonstrated using tourmaline, quartz, topaz, cane sugar and Rochelle salt (sodium potassium tartrate tetrahydrate). One year later, in 1881, Gabriel Lippmann found out that piezoelectric materials exhibit the reverse piezoelectric effect, meaning a deformation of the material when an electric field is applied [12]. Since then, intensive research has led to many applications like microbalances and scanning microscopy as examples for the direct piezoelectric effect, and motors and ultra-exact positioning as examples for the reverse piezoelectric effect.

Lead zirconate titanate (PZT) is the most commonly used piezoelectric material at the moment. Since the generators used throughout this work are made of PZT, the explanation of the physical basics is limited to this material. The elements of PZT (Pb, O, Ti/Zr) crystallize as perovskite crystals with the general formula $PbZr_{1-x}Ti_xO_3$. It has been shown that $x \approx 0.5$ maximizes the piezoelectric effect [22]. The piezoelectric effect is explained by means of Fig. 2.1. For temperatures below the Curie temperature ($T < T_C$), the charge center of the PZT crystallite moves away from the geometric center, leading to asymmetric electric dipoles with the characteristic rhomboedric/tetragonal structure. When the temperature is elevated above the Curie temperature ($T > T_C$), the crystallites are de-poled and the ceramic loses its piezoelectric characteristic.

Groups of dipoles with the same alignment are called Weiss domains. Due to the random distribution of Weiss domains with different alignment inside the ceramics as depicted in Fig. 2.2a, there is no macroscopic piezoelectric effect. Similar to the magnetizing of a permanent magnet, the ceramics can be polarized by applying a strong electric field, resulting in an arrangement of the Weiss domains as shown in Fig. 2.2b. The ceramic is now ready to use and exhibits piezoelectric properties, i.e.

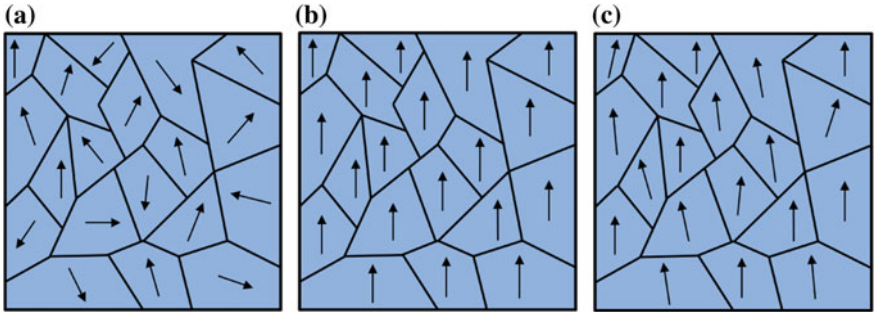

Fig. 2.2 Polarization of polycrystalline piezoelectric ceramic causes **a** the as-fired random domain polarity to align to **b** a net positive polarity, which **c** relaxes or ages over time

charges are generated at the top and bottom electrodes, inducing a current when a load is connected, or changing its shape when a voltage is applied. Fig. 2.2c shows a ceramic where the Weiss domains are slightly misaligned compared to the case shown in Fig. 2.2b due to exceeding the mechanical, thermal or electrical limits, or due to aging. This results in a reduction of the piezoelectric effect.

2.1.2 Constitutive Equations

The piezoelectric effect can be described using the coupled equations [2, 13]

$$\underline{S} = \underline{s}^E \cdot \underline{T} + \underline{d}^t \cdot \underline{E} \tag{2.1}$$

$$\underline{D} = \underline{d} \cdot \underline{T} + \underline{\varepsilon}^T \cdot \underline{E}, \tag{2.2}$$

where $\underline{S}$ is the mechanical strain, $\underline{T}$ is the mechanical stress, $\underline{D}$ is the electrical displacement (charge density), $\underline{E}$ is the electric field, $\underline{s}^E$ is the compliance under a zero or constant electrical field (indicated by the superscript E) and $\underline{\varepsilon}^T$ is the dielectric permittivity under a zero or constant stress (indicated by the superscript T). $\underline{d}$ and $\underline{d}^t$ are the matrices for the direct and the reverse piezoelectric effect, where the superscript t means the transposed matrix. Thus, (2.1) and (2.2) describe the reverse and the direct piezoelectric effect, respectively. Without the coupling term $\underline{d}^t \cdot \underline{E}$, (2.1) is simply Hooke's law relating strain and stress. Likewise, (2.2) is simply the dielectric equation when the coupling term $\underline{d} \cdot \underline{T}$ is neglected. The detailed matrix notation of (2.1) and (2.2) for a material of the 6 mm crystal class such as PZT ceramic is shown in (2.3) and (2.4):

$$\begin{bmatrix} S_1 \\ S_2 \\ S_3 \\ S_4 \\ S_5 \\ S_6 \end{bmatrix} = \begin{bmatrix} s_{11}^E & s_{12}^E & s_{13}^E & 0 & 0 & 0 \\ s_{12}^E & s_{11}^E & s_{13}^E & 0 & 0 & 0 \\ s_{13}^E & s_{13}^E & s_{33}^E & 0 & 0 & 0 \\ 0 & 0 & 0 & s_{44}^E & 0 & 0 \\ 0 & 0 & 0 & 0 & s_{44}^E & 0 \\ 0 & 0 & 0 & 0 & 0 & 2\left(s_{11}^E - s_{12}^E\right) \end{bmatrix} \begin{bmatrix} T_1 \\ T_2 \\ T_3 \\ T_4 \\ T_5 \\ T_6 \end{bmatrix} + \begin{bmatrix} 0 & 0 & d_{31} \\ 0 & 0 & d_{31} \\ 0 & 0 & d_{33} \\ 0 & d_{15} & 0 \\ d_{15} & 0 & 0 \\ 0 & 0 & 0 \end{bmatrix} \begin{bmatrix} E_1 \\ E_2 \\ E_3 \end{bmatrix} \tag{2.3}$$

$$\begin{bmatrix} D_1 \\ D_2 \\ D_3 \end{bmatrix} = \begin{bmatrix} 0 & 0 & 0 & 0 & d_{15} & 0 \\ 0 & 0 & 0 & d_{15} & 0 & 0 \\ d_{31} & d_{31} & d_{33} & 0 & 0 & 0 \end{bmatrix} \begin{bmatrix} T_1 \\ T_2 \\ T_3 \\ T_4 \\ T_5 \\ T_6 \end{bmatrix} + \begin{bmatrix} \varepsilon_{11}^T & 0 & 0 \\ 0 & \varepsilon_{11}^T & 0 \\ 0 & 0 & \varepsilon_{33}^T \end{bmatrix} \begin{bmatrix} E_1 \\ E_2 \\ E_3 \end{bmatrix} \tag{2.4}$$

The subscripts 1, 2 and 3 are related to the x, y and z axis in the cartesian coordinate system. Due to symmetrical reasons, many matrix elements are zero, and only few are independent. Generally, $\underline{D}$ and $\underline{E}$ are vectors, i.e. tensors of rank 1, and the permittivity $\underline{\varepsilon}^T$ is a tensor of rank 2. In principle, strain $\underline{S}$ and stress $\underline{T}$ are also tensors of rank 2, but due to the symmetry of the strain and stress tensors, the subscripts are conventionally re-labelled according to the so-called Voigt notation [13]: $11 \rightarrow 1$; $22 \rightarrow 2$; $33 \rightarrow 3$; $23 \rightarrow 4$; $13 \rightarrow 5$; $12 \rightarrow 6$. Thus, they can be written as vectors or rank-1 tensors in (2.3) and (2.4). Whereas the first three elements are related to the force applied on the surfaces perpendicular to the x, y and z direction, respectively, the other three elements denote shear forces. Due to the Voigt notation, the order of the compliance tensor $\underline{s}^E$ can be reduced from 4 to 2, resulting in the 6×6 matrix in (2.3).

2.2 Piezoelectric Harvester Design Configurations

Since this work focuses on piezoelectric material used in energy harvesting applications, the following explanations refer to the case where the piezoelectric material is used as a sensor rather than an actor. As shown in the constitutive (2.4), there are only three independent elements within the piezoelectric coupling tensor $\underline{d}$.

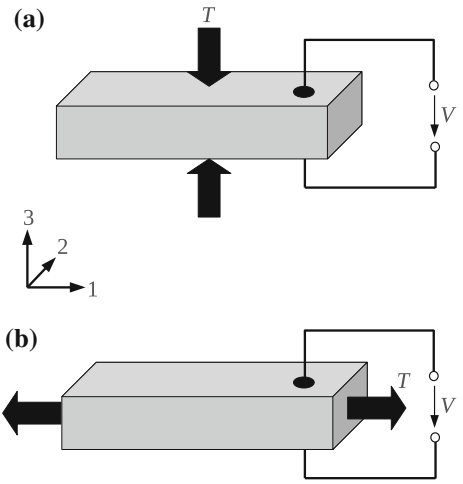

Fig. 2.3 Piezoelectric material operated in **a** 33 and **b** 31 mode

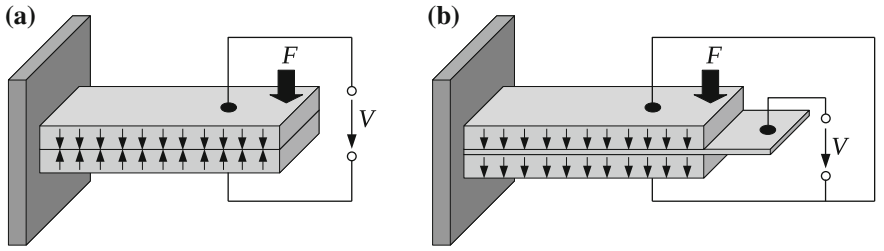

Fig. 2.4 Piezoelectric bimorph configured for **a** series and **b** parallel operation

Whereas d_{15} is related to shear stress which is not practical for energy harvesting, it is worth describing d_{33} and d_{31} more detailed.

Fig. 2.3 illustrates the two corresponding modes 33 and 31 in which piezoelectric material is generally used. The first number (3) indicates that the voltage is generated along the z axis in both modes, i.e. the electrodes are attached to the surfaces perpendicular to the z axis. The second numer indicates the direction of the applied stress. In 33 mode, the stress acts in the same direction as the voltage appears. When the piezoelectric material is operated in 31 mode, the stress is applied along the x axis, whereas the voltage appears in the z axis. For 31 mode, the constitutive (2.3) and (2.4) can be simplified to

$$\begin{cases} S_1 = s_{11}^E \cdot T_1 + d_{31} \cdot E_3 \\ D_3 = d_{31} \cdot T_1 + \varepsilon_{33}^T \cdot E_3. \end{cases} \tag{2.5}$$

The 31 mode is commonly used for energy harvesters, e.g. for bimorphs where two piezoelectric layers are attached together as shown in Fig. 2.4. When the cantilever

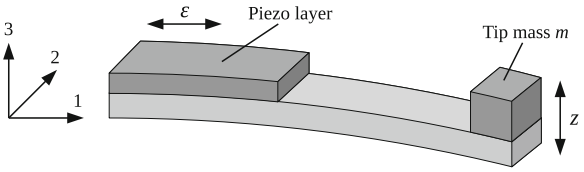

Fig. 2.5 Cantilever structure converting the displacement z in the 3 direction into a elongation ε in the 1 direction

bends down, the surfaces of the layers where the electrodes are attached are stretched and compressed for the top and the bottom electrode, respectively. The opposite characteristic can be observed for a cantilever bending upwards. When the two layers are poled in the opposite direction, the layers are connected in series. Thus, compared to one layer, the voltage doubles, the capacitance is divided in half, and the current stays the same. This situation is also shown in Fig. 2.4a. The parallel connection of the layers as illustrated in Fig. 2.4b is usually favored because the current and the capacitance are doubled whereas the voltage stays the same. Note that the type of layer connection only affects the voltage to current ratio, not the deliverable output power.

Piezoelectric material is usually very stiff (or low-compliant) resulting in very high, impractical resonant frequencies when it is attached directly to the frame. Thus, the cantilever configuration shown in Fig. 2.5 is commonly used where a large deflection z in the 3 direction is transformed into a small deformation ε in the 1 direction. This leads to a higher compliance, up-scaling the strain and lowering the resonant frequencies to the 100–200 Hz range according to the frequency spectrum of practical ambient vibrations. Often, a tip mass is added to the end of the beam, further increasing the compliance and the strain and thus decreasing the resonant frequency. Although the d_{31} coefficient correlating to the cantilever configuration is lower than the d_{33} coefficient ($d_{31} \approx 0.5 d_{33}$ for PZT [17]), the 31 mode configuration is usually preferred in energy harvesting applications due to these advantages.

2.3 Modeling of Kinetic Energy Harvesters

In this section, the modeling of the general vibration-based kinetic energy harvester is discussed, mainly corresponding to [9]. Besides the dependency of the excitation frequency, it is described how the transducer affects the characteristics of the system, and what is the upper limit for the extractable output power. In addition, the electrical equivalent circuit is presented, allowing the computer-aided simulation.

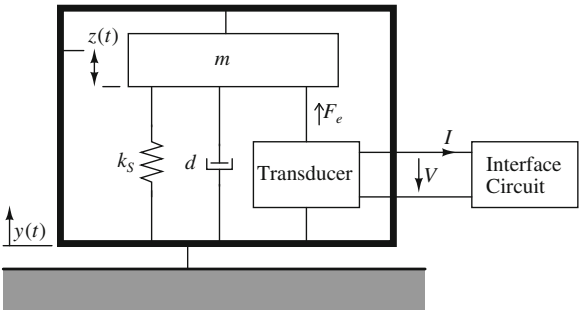

Fig. 2.6 Model of a kinetic energy harvester structure composed of lumped elements with connected electrical harvesting circuit

2.3.1 The General Mechanical Model of Kinetic Harvesters

Inetrial-based kinetic energy harvesters are modelled as second-order spring-mass-damper systems. The general model of kinetic energy harvesters was first developed by Williams and Yates [21]. Figure 2.6 shows the general model of a kinetic energy harvester composed of lumped elements with a transducer connected to an electrical interface circuit [14, 18, 21]. The frame represents the harvester which consists of a seismic mass m suspended on a spring with the stiffness k_S, generating a resonant spring-mass system. An external vibration which is assumed to exert a sinusoidal force on the harvester frame causes the frame to move harmonically with

$$y(t) = \widehat{y} \sin(\omega t),$$

where $\widehat{y}$ indicates the amplitude of the frame motion, and ω denotes the angular vibration frequency. The relative movement of the seismic mass m with respect to the frame is given by

$$z(t) = \widehat{z} \sin(\omega t + \varphi),$$

where $\widehat{z}$ indicates the amplitude of the mass motion, and φ points out that there is a phase difference between $y(t)$ and $z(t)$.

Mechanical damping due to friction, air resistance etc. is represented by the damper d. The movement of the mass can be used to deform a transducer, converting the mechanical energy into usable electrical energy. There are many possible conversion mechanisms, e.g. the capacitive, the inductive or the piezoelectric (see Sect. 1.1). Due to electromechanical feedback, the transducer exerts a restoring force F_e on the seismic mass if an interface circuit is connected, causing additional electrical damping d_e. The work which is done by the seismic mass against the restoring force is being converted into electricity.

2.3.2 Transfer Function

In order to derive the governing equation of the general kinetic energy harvester, it is assumed that the mass of the excitation source is much larger than m, so the excitation source is not damped by the energy harvester and thus it is assumed to provide infinite power. The force balance is given as

$$ma = m\ddot{z} + d\dot{z} + k_S z + F_e, \tag{2.6}$$

where

$$a(t) = \ddot{y}(t) = -\omega^2 \widehat{y} \sin(\omega t) = \widehat{a} \sin(\omega t)$$

indicates the acceleration acting on the harvester frame. So, ma represents the external force which is being exerted on the harvester frame. If the restoring force is considered as a damping force $F_e = d_e \dot{z}$, (2.6) can be rewritten as

$$ma = m\ddot{z} + (d + d_e)\,\dot{z} + k_S z. \tag{2.7}$$

In order to derive the transfer function, the Laplace transform of (2.7) is written as

$$ms^2 y = ms^2 z + (d + d_e)\,sz + k_S z. \tag{2.8}$$

Using the dimensionless terms for the mechanical and the electrical damping,

$$\zeta_d = \frac{d}{2m\omega_n} \quad \text{and} \quad \zeta_e = \frac{d_e}{2m\omega_n}, \tag{2.9}$$

where $\omega_n = \sqrt{\frac{k_S}{m}}$ denotes the natural frequency of the mechanical system, (2.8) can be rearranged to provide the transfer function

$$\frac{z(s)}{y(s)} = \frac{s^2}{s^2 + 2\omega_n\,(\zeta_d + \zeta_e)\,s + \omega_n^2}. \tag{2.10}$$

From (2.10), the displacement amplitude of the seismic mass can be derived as

$$\widehat{z}(\omega) = \frac{\frac{\omega}{\omega_n}\widehat{y}}{\sqrt{\left[1 - \left(\frac{\omega}{\omega_n}\right)^2\right]^2 + \left[2\,(\zeta_d + \zeta_e)\,\frac{\omega}{\omega_n}\right]^2}}. \tag{2.11}$$

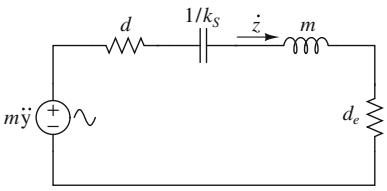

Fig. 2.7 Equivalent circuit of the kinetic harvester including electrical damping

2.3.3 Equivalent Circuit

The mechanical equivalent model discussed before is important for understanding the physical behavior of piezoelectric harvesters. However, since the the main scope of this work is the development of an interface circuit, an accurate electrical equivalent model of the harvester has to be found that can be used in simulation software like (P)Spice [11, 20] or Spectre [11]. Therefore, generally, a mechanical force can be represented as an electrical voltage, and a mechanical velocity (i.e. the first derivative of the displacement) can be replaced by an electric current [19]:

$$\begin{cases} I \triangleq \dot{z} \\ V \triangleq F \end{cases}. \tag{2.12}$$

Using this analogy, each term in (2.7) represents a voltage, and thus the electrical equivalent circuit as shown in Fig. 2.7 can be derived. The mass is represented as an inductor with the value m, the spring is modelled as a capacitor with the value $\frac{1}{k_S}$, and the mechanical and the electrical dampings are described by the resistors d and d_e. The voltage source $m\ddot{y} = ma$ models the external vibration. See Sect. 2.4.3 for a more detailed derivation of the lumped element values.

2.3.4 Output Power

The power dissipated in the transducer, i.e. in the resistor d_e, can now be calculated as follows:

$$P(\omega) = \frac{\left(\hat{\dot{z}}\right)^2}{2} d_e = \frac{(\omega\hat{z})^2}{2} d_e. \tag{2.13}$$

Using (2.11), equation (2.13) can be expanded as

$$P(\omega) = \frac{m\left(\frac{\omega}{\omega_n}\right)^3 \omega^3 \hat{y}^2 \zeta_e}{\left[1 - \left(\frac{\omega}{\omega_n}\right)^2\right]^2 + \left[2\left(\zeta_d + \zeta_e\right)\frac{\omega}{\omega_n}\right]^2}. \tag{2.14}$$

When the kinetic harvester is driven at resonance, i.e. $\omega = \omega_n$ holds, (2.14) simplifies to

$$P(\omega) = \frac{m\omega_n^3 \widehat{y}^2 \zeta_e}{4(\zeta_d + \zeta_e)^2}. \tag{2.15}$$

From (2.15), it can be calculated that the power dissipated in the transducer maximizes for $\zeta_e = \zeta_d$, which means that the mechanical damping equals the electrical damping. For this condition, (2.15) can be finally written as P_{lim}, representing the absolute maximum power extractable from a kinetic harvester:

$$P_{\text{lim}} = \frac{m\omega_n^3 \widehat{y}^2}{16\zeta_d},$$

or, written in terms of the mechanical damping $d = 2m\omega_n\zeta_d$ and the acceleration amplitude $\widehat{a} = \omega^2\widehat{y} = \omega_n^2\widehat{y}$:

$$P_{\text{lim}} = \frac{(m\widehat{a})^2}{8d}. \tag{2.16}$$

Sometimes, the quality factor Q is used instead of the damping ζ, where the two are related by $Q = \frac{1}{2\zeta}$. Thus, the quality factors due to mechanical and electrical damping can be expressed as

$$Q_d = \frac{1}{2\zeta_d} \quad \text{and} \quad Q_e = \frac{1}{2\zeta_e}, \tag{2.17}$$

and the total quality factor combining mechanical and electrical damping can be written as

$$\frac{1}{Q} = \frac{1}{Q_d} + \frac{1}{Q_e}.$$

Combining (2.9) and (2.17), the quality factors can also be expressed as

$$Q_d = \frac{m\omega_n}{d} \quad \text{and} \quad Q_e = \frac{m\omega_n}{d_e}. \tag{2.18}$$

Expression (2.16) points out that the maximum extractable output power only depends on the excitation force and the mechanical damping of the kinetic harvester. Since the maximum extractable output power is proportional to $\frac{1}{d}$, it seems desirable to try to keep the mechanical damping as low as possible in order to achieve a large output power. Decreasing the damping towards zero results in the maximum output power tending towards infinity, under the prerequisite that the input power provided by the excitation source is infinitely large. In terms of the quality factor, it seems

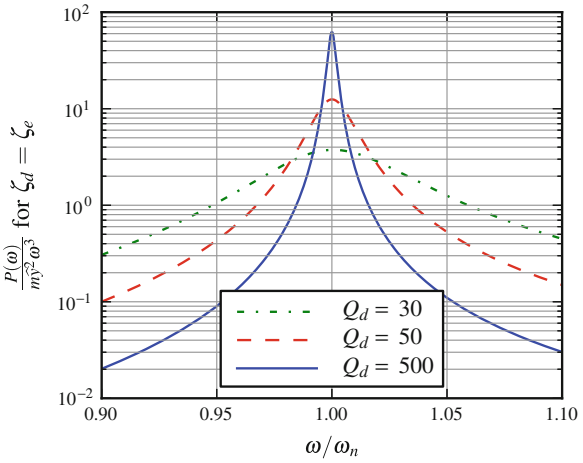

Fig. 2.8 Normalized maximum harvested power as a function of the excitation frequency, for different quality factors

desirable to achieve large values, as the quality factor and the damping are reciprocal to each other, see (2.17).

Fig. 2.8 illustrates the normalized power dissipated in the electrical damper, i.e. the harvested power, for different quality factors. As expected, the higher the quality factor, the larger the maximum extractable power, but the sharper the peak. This means that the resonant frequency of the harvester has to perfectly match the excitation frequency, otherwise the extractable power drops significantly.

2.4 Modeling of Piezoelectric Harvesters

In our case, the piezoelectric harvesting is of special interest, so this transducer mechanism will be investigated in detail in the following. The conclusions made in Sect. 2.3 are therefore taken as a reference.

2.4.1 Mechanical Modeling

Let's assume the piezoelectric material shown in Fig. 2.9. The force F acting on the material causes an elongation ε in the 1 direction. Using the relations

$$E = -\frac{V_P}{h} \qquad q = Dbl \qquad T = \frac{F}{bh} \qquad S = \frac{\varepsilon}{l} \qquad I = \frac{\partial q}{\partial t}, \tag{2.19}$$

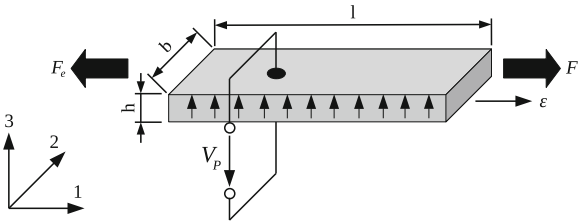

Fig. 2.9 Beam of piezo material used as energy harvester in the 31 mode

where q denotes the charge, the constitutive (2.5) can be rewritten in terms of the macroscopic variables F, ε, V and I instead of the local variables S, E, D and T [3]:

$$\begin{cases} F = k_P \varepsilon + \Gamma V_P \\ I = \Gamma \dot{\varepsilon} - C_P \dot{V}_P \end{cases} \tag{2.20}$$

where

$$k_P = \frac{bh}{l s_{11}^E} \qquad C_P = \left(\varepsilon_{33}^T - \frac{d_{31}^2}{s_{11}^E} \right) \frac{bl}{h} \qquad \Gamma = \frac{d_{31} b}{s_{11}^E}. \tag{2.21}$$

In (2.21), k_P denotes the stiffness of the piezoelectric material, C_P is the piezoelectric output capacitance, and Γ represents the generalized electromechanical coupling factor (GEMC) [16]. The first equation of (2.20) shows that the force F is composed of the "spring" force $k_P \varepsilon$ which depends on the material stiffness and the coupling force ΓV_P which depends on the voltage across the piezoelectric material. Due to the balance of forces, F can be considered as the restoring force F_e acting on the seismic mass, as defined in Fig. 2.6.

Usually, piezoelectric materials are very stiff, so very high resonant frequencies would result if the piezo beam would be suspended directly within the harvester frame. Thus, the cantilever configuration shown in Fig. 2.5 is preferred where a large deflection z in the 3 direction leads to a small elongation ε in the 1 direction. For this configuration, the constitutive (2.20) still hold [3], and hence they can be written as

$$\begin{cases} F_e = k_P z + \Gamma V_P \\ I = \Gamma \dot{z} - C_P \dot{V}_P \end{cases}, \tag{2.22}$$

and thus (2.6) can be written as

$$ma = m\ddot{z} + d\dot{z} + kz + \Gamma V_P, \tag{2.23}$$

where $k = k_P + k_S$ is the sum of the stiffnesses of the piezoelectric and the mechanical structure. This can be done under the assumption that a perfect bond exists between the beam and the piezoelectric material [8].

Finally, the spring mass damper system shown in Fig. 2.6 can be modelled by the differential equations

$$\begin{cases} ma &= m\ddot{z} + d\dot{z} + kz + \Gamma V_P \\ I &= \Gamma \dot{z} - C_P \dot{V}_P \end{cases}. \tag{2.24}$$

The energy balance of the vibration harvester system can be derived by multiplying (2.23) with the mass velocity $\dot{z}(t)$ and integrating over the time variable t [6]:

$$\underbrace{\int ma\dot{z}\ \mathrm{d}t}_{\text{total}} = \underbrace{\frac{1}{2}m\dot{z}^2}_{\text{kinetic}} + \underbrace{\int d\dot{z}^2\,\mathrm{d}t}_{\text{damping}} + \underbrace{\frac{1}{2}kz^2}_{\text{elastic}} + \underbrace{\int \Gamma V_P \dot{z}\,\mathrm{d}t}_{\text{electrical}} \tag{2.25}$$

where

$$\int \Gamma V_P \dot{z}\,\mathrm{d}t = \frac{1}{2}C_P V_P^2 + \int V_P I\,\mathrm{d}t. \tag{2.26}$$

Expression (2.25) states that the energy injected into the system is composed of the kinetic energy, the mechanical damping losses, the elastic energy and the energy converted into electrical energy. According to (2.26), the energy converted into electrical energy is separated into the energy stored on the piezoelectric capacitance and the energy absorbed by the electrical load. The latter energy is the part which is actually being harvested.

2.4.2 Electromechanical Coupling and Damping

The piezoelectric coupling factor is an important parameter because it is a measure for the part of injected mechanical energy which is converted into electrical energy. High coupling means that a large amount of energy can be harvested from a given environmental mechanical energy, i.e. the last term in (2.25) is large. Vice versa, the same mechanical energy leads to only little useable eletrical energy for a lowly coupled harvester. Since the actuator piezoelectric effect is present in the reverse direction, an electrical load drawing power out of the harvester induces a feedback on the deflection of the piezoelectric beam which induces electrical damping, corresponding to d_e as defined in Sect. 2.3.1. This means that a highly coupled piezoelectric harvester is damped more intensely than a lowly coupled one. Hence, the coupling factor is of outstanding importance because it determines whether the SECE technique discussed in this book extracts more power out of a piezoelectric harvester compared to a standard bridge rectifier.

For the piezoelectric beam shown in Fig. 2.9, according to the IEEE Standard on Piezoelectricity [13], the squared coupling factor is given by

$$k_{31}^2 = \frac{d_{31}^2}{\varepsilon_{33}^T s_{11}^E}. \tag{2.27}$$

Note that k_{31}^2 exclusively depends on piezoelectric material properties. The measured squared material coupling factor k_{31}^2 has been reported to be up to 0.7 [3]. In order to link the *material* coupling factor k_{31}^2 and the *generalized electromechanical* coupling factor (GEMC) Γ which depends on the geometry of the used cantilever as defined in (2.21), (2.27) can be expressed as

$$k_{31}^2 = \frac{\Gamma^2}{k_P C_P}.$$

In order to describe the total harvester structure (e.g. the resonator geometry) instead of the piezoelectric layer properties, the *effective* coupling factor can be used [13]:

$$k_{\text{eff}}^2 = \frac{\omega_{\text{oc}}^2 - \omega_{\text{sc}}^2}{\omega_{\text{oc}}^2}, \tag{2.28}$$

where ω_{oc} and ω_{sc} denote the angular resonance frequency of the open-circuited and short-circuited structure, respectively. The effective coupling factor is a convenient parameter allowing to compare different harvesting structures using any piezoelectric material. According to [6, 15], realistic values of k_{eff}^2 are in the range of 0.01–0.1.

Due to the electromechanical feedback, two resonant frequencies exist for the piezoelectric harvester, depending on the electrical loading. The fundamental resonance frequency is determined for the case that the piezoelectric harvester terminals are short-circuited:

$$\omega_{\text{sc}} = \sqrt{\frac{k}{m}}. \tag{2.29}$$

The anti-resonance frequency is higher than the fundamental resonance frequency and shows at open circuit configuration:

$$\omega_{\text{oc}} = \omega_{\text{sc}}\sqrt{1 + k_{\text{eff}}^2}.$$

To avoid confusion, it is emphasized that k denotes the total stiffness composed of the mechanical structure and the piezoelectric material, whereas k_{eff}^2 indicates the squared effective electromechanical coupling factor. For both the fundamental and anti-resonance frequency, the electromechanical damping exerted by the respective electrical load (i.e. $R_L = 0$ for the fundamental frequency and $R_L = \infty$ for the anti-resonance frequency) is zero [4].

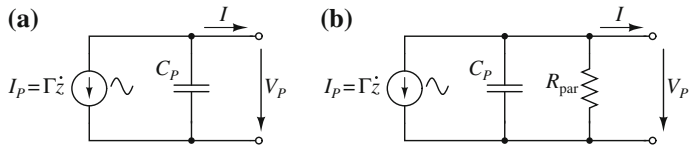

Fig. 2.10 Uncoupled equivalent circuit of the piezoelectric harvester **a** neglecting and **b** considering the dielectric losses

The following equation correlates the GEMC to the effective electromechanical coupling factor [16, 18]:

$$k_{\text{eff}}^2 = \frac{\Gamma^2}{kC_P}. \tag{2.30}$$

For the equivalent circuits presented in the following, the GEMC Γ will be used in order to describe the coupling phenomenon.

2.4.3 Equivalent Circuits

As a first approach, the second equation of (2.24) can be converted into the uncoupled electrical equivalent circuit indexUncoupled electrical equivalent circuit shown in Fig. 2.10a [1, 18]. The sinusoiodal current source represents the vibrating beam with $I_P = \Gamma\dot{z}$, and the piezoelectric output capacitance is modelled by C_P. By means of (2.11), the amplitude of the current source $\widehat{I}_P$ can be expressed in terms of the external acceleration $\widehat{a} = \widehat{\ddot{y}}$ and several generator parameters as follows:

$$\widehat{I}_{P,\text{oc}} = \widehat{a} \cdot \frac{\Gamma \cdot m}{d}, \tag{2.31}$$

assuming excitation at resonance (i.e. $\omega = \omega_n$) and no load (i.e. $\zeta_e = 0$). For the Synchronous Electric Charge Extraction (SECE) technique which is the basic principle of the proposed interface circuit (see Sect. 3.3), in a first approximation it can be assumed that $\zeta_e = \zeta_d$, and hence the following equation holds at resonance:

$$\widehat{I}_{P,\text{SECE}} = \widehat{a} \cdot \frac{\Gamma \cdot m}{2d}. \tag{2.32}$$

The voltage across the piezoelectric terminals is indicated by V_P . As depicted in Fig. 2.10b, sometimes the resistor R_{par} is added to consider the dielectric losses since the piezoelectric capacitance is not a perfect insulator. Since R_{par} is usually very high (>10 MΩ), it is neglected throughout this book. This equivalent circuit completely neglects the mechanical resonator structure, but it is sufficient for the

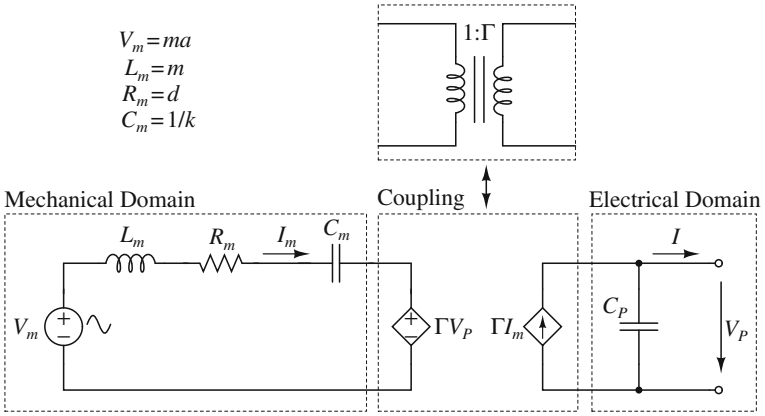

Fig. 2.11 Coupled electromechanical equivalent circuit of the piezoelectric harvester [10, 16] (The controlled sources are sometimes replaced by a transformer.)

design process of interface circuits, where it is irrelevant which external vibration force generates the actual voltage across the piezoelectric terminals.

However, if the feedback of the interface circuit on the piezoelectric harvester or an accurate prediction of the output power for a given vibration acceleration is important, a more sophisticated electrical equivalent circuit has to be found. According to (2.12), the mechanical velocity $\dot{z}$ can be represented by an electrical current:

$$\dot{z} := I_m ,$$

and hence the differential (2.24) can be rewritten as:

$$\begin{cases} ma &= m\dot{I}_m + dI_m + k\int I_m \,\mathrm{d}t + \Gamma V_P \\ I &= \Gamma I_m - C_P \dot{V}_P \end{cases} . \tag{2.33}$$

Note that each term in the first equation of (2.33) can now be represented as an electrical voltage instead of a mechanical force, as stated in (2.12). Thus, the coupled electrical equivalent circuit composed of lumped elements, as shown in Fig. 2.11, can be derived [10, 16]. The electrical domain is a representation of the second equation of Fig. 2.33, so the value of the capacitor can be directly defined as C_P. An additional parallel resistor modelling the leakage losses is omitted since its resistance is usually very high ($>10\,\mathrm{M\Omega}$).

A little more effort has to be made in order to determine the lumped element parameters of the electrical domain. Therefore, the method of equating the coefficients between the first equation of (2.33) and the Kirchhoff Voltage Law (KVL) of the mechanical domain is applied:

$$V_m = L_m \dot{I}_m + R_m I_m + \frac{1}{C_m}\int I_m \,\mathrm{d}t + \Gamma V_P .$$

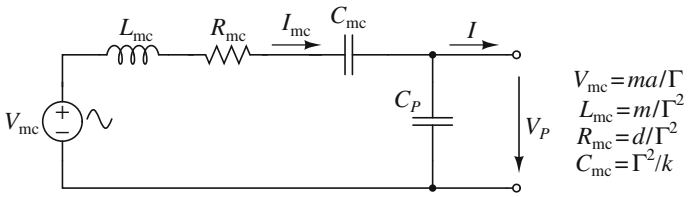

Fig. 2.12 Simplified electromechanical equivalent circuit of the piezoelectric harvester, where the coupling factor is considered in the lumped element parameters

As a result, the mass is modeled by an inductor with inductance $L_m = m$, the stiffness of the piezoelectric beam is represented by a capacitor with capacitance $C_m = 1/k$, the parasitic damping is modeled by a resistor with resistance $R_m = d$, and the alternating input force is modeled as a voltage source $V_m = m\ddot{y} = ma$. Controlled voltage and current sources using the GEMC (see Sect. 2.4.1) are used to couple the mechanical and the electrical domain, alternatively a transformer with the winding ratio $1 : \Gamma$ often found in literature has equal functionality.

Finally, the controlled sources/the transformer can be eliminated as shown in Fig. 2.12, simplifying mathematical calculation. Therefore, the first equation of (2.33) is multiplied by $\frac{\Gamma}{\Gamma^2}$:

$$\begin{cases} \frac{ma}{\Gamma} &= \frac{m}{\Gamma^2}\Gamma\dot{I}_m + \frac{d}{\Gamma^2}\Gamma I_m + \frac{k}{\Gamma^2}\Gamma\int I_m \,\mathrm{d}t + V_P \\ I &= \Gamma I_m - C_P\dot{V}_P \end{cases}. \tag{2.34}$$

Now, introducing the new symbol

$$I_{mc} = \Gamma I_m,$$

and performing the method of equating the coefficients between (2.34) and the KVL of the simplified equivalent circuit:

$$V_{mc} = L_{mc}\dot{I}_{mc} + R_{mc}I_{mc} + \frac{1}{C_{mc}}\int I_{mc}\,\mathrm{d}t + V_P,$$

the lumped element parameters of the simplified equivalent circuit are given by

$$V_{mc} = \frac{ma}{\Gamma} \qquad L_{mc} = \frac{m}{\Gamma^2} \qquad R_{mc} = \frac{d}{\Gamma^2} \qquad C_{mc} = \frac{\Gamma^2}{k}. \tag{2.35}$$

Both the equivalent circuits shown in Figs. 2.11 and 2.12 accurately model the electromechanical feedback, i.e. the resonance frequency shift and the piezoelectric voltage change if an electrical load is connected (see also Sect. 2.4.2). However, the simulation time using these equivalent circuits can be long since a startup oscillation takes place until the steady state is found. Since the accurate behavior of the

piezoelectric harvester in terms of feedback is rather unimportant for the design of the interface circuitry, the basic model shown in Fig. 2.10 can be used during the design process. The simulation time using the simple model is much shorter than using the complex model since no steady state has to be found. Hereby, the excitation is modeled by a sinusoidal current source which represents the vibrating beam. In most cases, it is sufficient to set its current amplitude such that a desired piezoelectric voltage is generated. For the design of the proposed Pulsed Synchronous Charge Extractor (PSCE) interface circuit, the current amplitude can be calculated using (2.32). The piezoelectric capacitance should have a somehow realistic value since it determines how much energy can be extracted from the harvester during one transfer cycle.

After the successful chip design and fabrication, it may be interesting to know how the chip performs connected to different piezoelectric harvesters, especially in terms of the power that can be extracted. For that reason, it is important to have an accurate model that behaves similar to a real piezoelectric harvester.

2.4.4 Maximum Output Power

The main figure of merit of interface circuits for any kind of generator is the power which they are able to extract. Therefore, it is helpful to know the absolute maximum power which can be extracted from the harvester. Although this is only a theoretical value which cannot be achieved in real applications, it is nevertheless a means for classifying the actual extracted power.

Basically, a generator with internal impedance Z outputs a maximum power if it is terminated by a load impedance equal to its conjugate complex impedance $\overline{Z}$. Using the simplified model from Fig. 2.12, the internal impedance of a piezoelectric harvester is given as

$$Z = \frac{1}{j\omega C_P + \dfrac{1}{R_{\mathrm{mc}} + \frac{1}{j\omega C_{\mathrm{mc}}} + j\omega L_{\mathrm{mc}}}}.$$

By substituting the imaginary j by $-j$, the conjugate complex impedance can be written as

$$\overline{Z} = \frac{1}{-j\omega C_P + \dfrac{1}{R_{\mathrm{mc}} - \frac{1}{j\omega C_{\mathrm{mc}}} - j\omega L_{\mathrm{mc}}}}.$$

Thus, in order to get an electrical equivalent circuit representing $\overline{Z}$, each capacitor within Z has to be substituted by an inductor and vice versa, leading to the equivalent circuit shown in Fig. 2.13. The conjugate complex pair $C_P - \overline{L}_P$ represents an infinitely high impedance, and the other pairs $C - \overline{L}$ and $L - \overline{C}$ create a zero impedance,

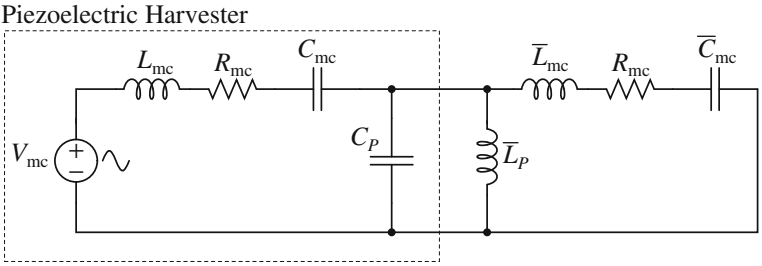

Fig. 2.13 Piezoelectric model with conjugate complex load

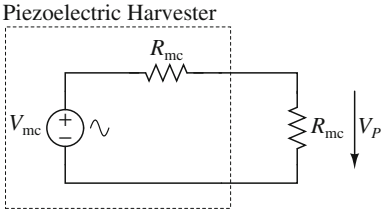

Fig. 2.14 Simplified piezoelectric model with conjugate complex load

if the values of the load impedance components are set as follows:

$$\overline{L}_P = \frac{1}{\omega^2 C_P} \qquad \overline{L}_{mc} = \frac{1}{\omega^2 C_{mc}} \qquad \overline{C}_{mc} = \frac{1}{\omega^2 L_{mc}}. \tag{2.36}$$

In this case, the circuit from Fig. 2.13 reduces to the circuit depicted in Fig. 2.14, which represents a simple resistive voltage divider. The root mean square power dissipated at the load resistor represents the maximum extractable power, and it can be calculated as

$$P_{lim} = \frac{V_{P,rms}^2}{R_{mc}} = \frac{\left(\frac{0.5\widehat{V}_{mc}}{\sqrt{2}}\right)^2}{R_{mc}}, \tag{2.37}$$

where $V_{P,rms}$ indicates the root mean square voltage at the load resistor, and $\widehat{V}_{mc}$ denotes the amplitude of the voltage source V_{mc}. For $\widehat{V}_{mc} = m\widehat{a}/\Gamma$ and $R_{mc} = d/\Gamma^2$ as given in (2.35), (2.37) can be finally expressed as

$$P_{lim} = \frac{(m\widehat{a})^2}{8d}. \tag{2.38}$$

Note that the derivation of P_{lim} shown above and the derivation based on the mechanics of kinetic harvesters explored in Sect. 2.3.4 lead to identical (2.38) and (2.16).

References

1. J. Ajitsaria, S.Y. Choe, D. Shen, D.J. Kim, Modeling and analysis of a bi-morph piezoelectric cantilever beam for voltage generation. Smart Mater. Struct. **16**, 447–454 (2007)
2. D. Damjanovic, Ferroelectric, dielectric and piezoelectric properties of ferroelectric thin films and ceramics. Rep. Prog. Phys. **61**, 1267 (1998)
3. R. D'hulst, in Power processing circuits for vibration-based energy Har- vesters. Ph.D. thesis, KU Leuven 2009
4. N.E. DuToit, B.L. Wardle, Experimental verification of models for microfabricated piezoelectric vibration energy harvesters. AIAA J. **45**(5), 1126–1137 (2007)
5. G. Gautschi, in *Piezoelectric Sensorics: Force, Strain, Pressure, Accelera- tion and Acoustic Emission Sensors, Materials and Amplifiers* (Springer Verlag, 2002)
6. D. Guyomar, A. Badel, E. Lefeuvre, C. Richard, Toward energy harvest- ing using active materials and conversion improvement by nonlinear process- ing. IEEE Trans. Ultrason., Ferroelectrics Freq. Control **52**(4), 584–595 (2005)
7. B. Jaffe, in Piezoelectric Ceramics. (Academic Press, Waltham, 1971)
8. A. Kasyap , J. Lim, D. Johnson , S. Horowitz, T. Nishida, K. Ngo, M. Sheplak , L. Cattafesta, in *Energy Reclamation from a Vibrating Piezoceramic Com- posite Beam*, in *Proceedings of 9th International Congress on Sound and Vibration*, Orlando, FL, USA, vol 9, 8–11 July 2002, pp. 36–43
9. T. Kazmierski, in Energy Harvesting Systems: principles, Modeling and Applications. (Springer Verlag 2010)
10. N. Kong, D.S. Ha, A. Erturk, D.J. Inman, Resistive impedance matching circuit for piezoelectric energy harvesting. J. Intell. Mater. Syst. Struct. **21**(13), 1293–1302 (2010)
11. K. Kundert, in *The Designer's Guide to SPICE and SPECTRE*. (Kluwer Academic Publishers 1995)
12. G. Lippmann, in Principe de la conservation de l'électricité, ou second principe de la théorie des phènomènes électriques. Annales de Chimie et de Physique **24**, 145 (1881)
13. A.H. Meitzler, H.F. Tiersten, A.W. Warner, D. Berlincourt, G.A. Couqin, F.S. Welsh III, IEEE Standard on Piezoelectricity. Institute of Electrical and Elec- tronics Engineers (IEEE), New York (1988)
14. P.D. Mitcheson, T.C. Green, E.M. Yeatman, A.S. Holmes, Architectures for vibration-driven micropower generators. J Microelectromech Syst **13**(3), 429–440 (2004)
15. M. Renaud, T. Sterken, A. Schmitz, P. Fiorini, C. Van Hoof, R. Puers, in *Piezoelectric Harvesters and MEMS Technology: Fabrication, Modeling and Measurements*, in *Proceedings of the International Conference on Solid- State Sensors, Actuators and Microsystems (Transducers)*, Lyon, France, 10–14 June 2007, pp. 891–894
16. M. Renaud, K. Karakaya, T. Sterken, P. Fiorini, C. Van Hoof, R. Puers, Fabrication, modelling and characterization of MEMS piezoelectric vibration harvesters. Sens. Actuators A: Phys. **145**, 380–386 (2008)
17. S. Roundy, P. Wright, J. Rabaey, in *Energy scavenging for wireless sensor networks: with special focus on vibrations*. (Kluwer Academic Publishers 2004))
18. Y.C. Shu, I.C. Lien, Analysis of power output for piezoelectric energy harvesting systems. Smart Mater. Struct. **15**, 1499 (2006)
19. H.A.C. Tilmans, Equivalent circuit representation of electromechanical transducers: I. Lumped-parameter systems. J. Micromech. Microeng. **6**, 157 (1996)
20. P.W. Tuinenga, in *SPICE: a guide to circuit simulation and analysis using PSpice*. (Prentice Hall PTR 1995)
21. C.B. Williams, R.B. Yates, Analysis of a micro-electric generator for microsystems. Sens. Actuators A: Phys. **52**(1–3), 8–11 (1996)
22. Y. Xu, X. Yuhuan, *Ferroelectric Materials Applications* (North- Holland Elsevier, Netherlands, 1991)

http://www.springer.com/978-94-017-9287-5

CMOS Circuits for Piezoelectric Energy Harvesters
Efficient Power Extraction, Interface Modeling and Loss Analysis
Hehn, T.; Manoli, Y.
2015, XVII, 204 p. 137 illus., Hardcover
ISBN: 978-94-017-9287-5